

blood

2011 117: 4142-4153
Prepublished online February 9, 2011;
doi:10.1182/blood-2010-09-307538

Conditional HIF-1 induction produces multistage neovascularization with stage-specific sensitivity to VEGFR inhibitors and myeloid cell independence

Sunday S. Oladipupo, Song Hu, Andrea C. Santeford, Junjie Yao, Joanna R. Kovalski, Ralph V. Shohet, Konstantin Maslov, Lihong V. Wang and Jeffrey M. Arbeit

Updated information and services can be found at:
<http://bloodjournal.hematologylibrary.org/content/117/15/4142.full.html>

Articles on similar topics can be found in the following Blood collections
[Vascular Biology](#) (249 articles)

Information about reproducing this article in parts or in its entirety may be found online at:
http://bloodjournal.hematologylibrary.org/site/misc/rights.xhtml#repub_requests

Information about ordering reprints may be found online at:
<http://bloodjournal.hematologylibrary.org/site/misc/rights.xhtml#reprints>

Information about subscriptions and ASH membership may be found online at:
<http://bloodjournal.hematologylibrary.org/site/subscriptions/index.xhtml>



Conditional HIF-1 induction produces multistage neovascularization with stage-specific sensitivity to VEGFR inhibitors and myeloid cell independence

*Sunday S. Oladipupo,¹ *Song Hu,² Andrea C. Santeford,¹ Junjie Yao,² Joanna R. Kovalski,¹ Ralph V. Shohet,³ Konstantin Maslov,² Lihong V. Wang,^{2,4} and Jeffrey M. Arbeit^{1,4}

¹Urology Division, Department of Surgery, ²Department of Biomedical Engineering, and ³Department of Medicine, University of Hawaii, Honolulu, HI; and ⁴Siteman Cancer Center, Washington University, St Louis, MO

Neovascularization is a crucial component of tumor growth and ischemia. Although prior work primarily used disease models, delineation of neovascularization in the absence of disease can reveal intrinsic mechanisms of microvessel regulation amenable to manipulation in illness. We created a conditional model of epithelial HIF-1 induction in adult mice (TetON-HIF-1 mice). Longitudinal photoacoustic microscopy (L-PAM) was coincidentally developed for noninvasive, label-free serial imaging of red blood cell-perfused vasculature in the same mouse for weeks to months. TetON-HIF-1 mice

evidenced 3 stages of neovascularization: development, maintenance, and transgene-dependent regression. Regression occurred despite extensive and tight pericyte coverage. L-PAM mapped microvascular architecture and quantified volumetric changes in neocapillary morphogenesis, arteriovenous remodeling, and microvessel regression. Developmental stage endothelial proliferation downregulation was associated with a DNA damage checkpoint consisting of p53, p21, and endothelial γ -H2AX induction. The neovasculature was temporally responsive to VEGFR2 immuno-blockade,

with the developmental stage sensitive, and the maintenance stage resistant, to DC101 treatment. L-PAM analysis also pinpointed microvessels ablated or resistant to VEGFR2 immuno-blockade. HIF-1–recruited myeloid cells did not mediate VEGFR2 inhibitor resistance. Thus, HIF-1 neovascularization in the absence of disease is self-regulated via cell autonomous endothelial checkpoints, and resistant to angiogenesis inhibitors independent of myeloid cells. (*Blood*. 2011;117(15):4142-4153)

Introduction

Neovascularization is a process whereby new vessels are created and existing ones remodeled to supply growing or ischemic tissues with oxygen and nutrients. Although numerous studies have been performed in preclinical tumor or ischemia models, determination of the mechanisms of angiogenesis and neovascularization regulation in the absence of disease could provide insight into endothelial cell signaling and stromal cell trafficking otherwise obscured by a microenvironment altered by illness.

Neovascularization is an adult developmental program that unfolds over time, induced by a collection of angiogenic factors. However, preclinical studies of neovascularization have focused on one or a few time points in what is a continuous process, or have used vectors transiently expressing elevated levels of angiogenic factors.¹ Adult neovascularization and stromal remodeling in the absence of disease were studied using Tet-inducible vascular endothelial growth factor (VEGF).² However, because of the inaccessibility of organs targeted for VEGF gain of function, liver and heart, neovascular development was not studied using day-to-day analysis after transgene activation. Moreover, these organs possessed a tissue cellular organization that made spatial analysis between transgene broadcasting and receiving vascular cells challenging. Another strategy for conditional adult neovascular induction was cell autonomous regulation, within the endothelial cell itself. There, high-level transgenic overexpression of constitutive

myristoylated AKT produced marked alterations of microvessel structure and stromal edema; however, the kinetics of neovascular development was not investigated.³

Neovascularization is also ideally suited to serial imaging. Elegant studies delineated alterations of both the microvasculature and the microenvironment using optical microscopy techniques, such as single-photon or multiphoton fluorescence microscopy and Doppler optical coherence tomography.⁴ However, challenges with such pure optical techniques included the requirement for repeated fluorescent dye injections, the need for tissue window construction, or the necessity for blood flow.^{5,6}

In most instances, neovascularization in disease is coordinated by induction of the hypoxia-inducible factor (HIF) family, primarily HIF-1 and HIF-2.⁷ These transcription factors are heterodimers of an oxygen-labile HIF-1 or HIF-2 α subunit, each paired with the same stable HIF- β subunit. Oxygen instability is mediated by prolyl hydroxylase catalyzed hydroxylation of proline residues within the oxygen-dependent degradation domain.⁸ Nonhypoxic HIF- α induction is produced by enhanced HIF mRNA translation controlled by phosphatidylinositol 3-kinase-mammalian target of rapamycin pathway activation.⁹ HIF-1 and HIF-2 induce expression of multiple angiogenic factors.¹⁰ HIFs signal angiogenesis via paracrine,¹¹ autocrine,¹² and endocrine mechanisms.¹³ HIF-1 and HIF-2 α protein overexpression has been documented in human

Submitted September 23, 2010; accepted January 18, 2011. Prepublished online as *Blood* First Edition paper, February 9, 2011; DOI 10.1182/blood-2010-09-307538.

*S.S.O. and S.H. contributed equally to this study.

The online version of this article contains a data supplement.

The publication costs of this article were defrayed in part by page charge payment. Therefore, and solely to indicate this fact, this article is hereby marked "advertisement" in accordance with 18 USC section 1734.

© 2011 by The American Society of Hematology

ischemic tissues and organs, high-grade premalignant lesions, and cancers.^{7,9} HIF-1 α expression levels are also prognostic in clinical malignancies.⁹ Previously, we reported that germline transgenic expression of a HIF-1 α oxygen-dependent degradation domain mutant in skin produced hypervascularity with microvessels of normal morphology. However, the vasculature in that model was quiescent, lacking endothelial proliferation, angiogenesis, or microvascular network growth over time.¹¹

Here we deployed a conditional expression strategy to create a disease-free model of HIF-1 induction in adult epithelium. We targeted a doxycycline (DOX)-regulated, oxygen-insensitive HIF-1 α transgene to mouse skin (TetON-HIF-1 mice). HIF-1 activation produced 3 stages of neovascularization: development, maintenance, and transgene-dependent regression. Surprisingly, endothelial proliferation was cell autonomously down-regulated by a DNA damage checkpoint despite persistent VEGFR2 activation. Moreover, myeloid cells recruited to the skin stroma contributed to neither neovascularization nor VEGF inhibitor resistance. Photoacoustic microscopy (PAM) longitudinally imaged and determined microcirculatory dynamics during neovascular network development, transgene-dependent regression, and stage-specific angiogenic inhibitor responsiveness. The preclinical TetON-HIF-1 model and longitudinal photoacoustic microscopy (L-PAM) technology are promising tools for studying angiogenesis and the microenvironment as they are altered during neovascularization.

Methods

Mouse procedures

K5-rtTA “TetOn” driver transgenic mice, created using FVB/n embryo microinjection, were obtained from Adam Glick at Pennsylvania State University.¹⁴ TRE-human-HIF-1 α ^{P402A/P564A/N803A} transgenic mice, in the C57Bl6 background, were obtained from Ralph Shohet and Rick Bruick at University of Texas Southwestern (Dallas, TX).¹⁵ Use of the HIF-1 α ^{P402A/P564A/N803A} mutant blocked oxygen-dependent hydroxylation of proline and asparagine residues, producing a protein that was resistant to VHL-mediated proteasomal degradation and transcriptional repression.⁸ All experiments were performed in heterozygous double-transgenic mice, designated “TetON-HIF-1” in the manuscript and “DTG” in the figures, genotyped by tail DNA polymerase chain reaction performed with primers specific for both K5 and TRE-human-HIF-1 α ^{P402A/P564A/N803A} transgenes. Nontransgenic (NTG), single transgenic (NTG/TG), and transgenic DOX day 0 TetON-HIF-1 mice served as controls. Serial intercrossing of TRE-HIF-1 mice with K5-rtTA partners progressively bred this background into FVB/n (n = 10). DOX chow (200 mg/kg) was commercially obtained (S3888; Bio-Serv) and provided ad libitum for transgene induction. All animal care and experimental procedures were carried out in conformance with the laboratory animal protocol approved by the School of Medicine Animal Studies Committee of Washington University, St Louis.

Tissue harvest, fixation, and preparation for microscopy

DOX-treated TetON-HIF-1 and control mice or baseline DOX day 0 TetON-HIF-1 mice were anesthetized with 2.5% Avertin, and one ear was removed and fixed in ice-cold 70% ethanol overnight at 4°C. Mice were then perfused with either 10% buffered formalin or 4% paraformaldehyde via the left ventricle. Ethanol- and formalin-fixed ears were paraffin-embedded and 5- μ m sections obtained for both immunofluorescent and histologic analyses. Paraformaldehyde-fixed ears were placed in optimal cutting temperature media, frozen on dry ice, and 10- μ m sections were stained with hematoxylin/eosin or toluidine blue (mast cell staining).

Ear whole mounts were processed from mice perfused with either fluorescein isothiocyanate (FITC)-conjugated *Lycopersicon esculentum*

lectin (FITC-Lectin, 100 μ g, L-1171; Vector Laboratories) or *Griffonia simplicifolia* I isolectin B4 (50 μ g, 121413; Invitrogen) as described previously.¹¹ Details of thin and whole-mount ear tissue microscopy are available in supplemental Methods (available on the *Blood* Web site; see the Supplemental Materials link at the top of the online article).

Immunostaining

Tissue section preparations, antibody sources, and working dilutions are described in detail in supplemental Methods.

Endothelial cell proliferation and apoptosis determination

5-Bromo-2'-deoxyuridine (B5002; Sigma-Aldrich), 1 mg/10 g mouse in 0.8% saline was injected intraperitoneally, and mice were killed 4 hours later. Ears were harvested and fixed in 70% ethanol, and deparaffinized and rehydrated. Further details of 5-bromo-2'-deoxyuridine immunofluorescence are described in supplemental Methods. Apoptotic endothelial cells were visualized using dual MECA32/cleaved caspase-3 (1:1000; Cell Signaling) immunofluorescence on formalin-fixed, paraffin-embedded sections after acid citrate, pH 6.0, antigen retrieval in a pressure cooker (Biocare Medical).

Quantification of microvessel density, pericyte coverage, proliferating and apoptotic endothelial cells

Quantification of vascular density and proliferating or apoptotic endothelial cells are described in detail in supplemental Methods.

Total RNA isolation and real-time reverse-transcribed-polymerase chain reaction analysis

Total RNA was isolated from ears using TRIzol (15596-018; Invitrogen). Details of the reverse-transcribed polymerase chain reaction methods are in supplemental Methods, whereas primer-probe set sequences are displayed in supplemental Table 1.

Nuclear extract preparation

HIF-1 α protein levels were determined in nuclear extracts of NTG and TetON-HIF-1 ear tissue homogenates as described previously.¹⁶ Protein bands were quantified by densitometry, and protein loading normalized to Sp1 (554129; BD Biosciences).

Western blotting

Tissues were lysed in RIPA buffer: 50mM Tris (pH 7.4), 150mM NaCl, 1mM ethylenediaminetetraacetic acid, 1% NP-40, 0.1% sodium dodecyl sulfate, 1% sodium deoxycholate, 1% Triton X-100, freshly added 2% Protease Inhibitor Cocktail (P8340; Sigma-Aldrich), and Phosphatase Inhibitor Cocktail I and II (P2850 and P5726; Sigma-Aldrich). Immunoblotting was performed using 120 μ g of protein extract. Details on immunoblotting and antibodies are provided in supplemental Methods.

VEGF, PIGF, and SDF-1 α ELISA

VEGF, placental growth factor (PIGF), and stromal derived factor-1 α (SDF-1 α) tissue and plasma protein levels in TetON-HIF-1 and NTG ear skin homogenates or blood plasma were determined by enzyme-linked immunosorbent assay (ELISA; MMV00, MP200, and MCX120; R&D Systems) according to the manufacturer's protocol. Details are provided in supplemental Methods.

Immunoblocking antibodies

For VEGFR2 or VEGFR1 immuno-blockade, 800 μ g of DC101, MF1 (generous gifts from ImClone Systems), or nonspecific rat IgG (012-000-003; Jackson ImmunoResearch Laboratories) were administered intraperitoneally 3 times per week starting on day 0 or day 14 of DOX induction of TetON-HIF-1 or DOX-treated NTG controls. After treatment, mice were either anesthetized for noninvasive L-PAM imaging or lectin-perfused,

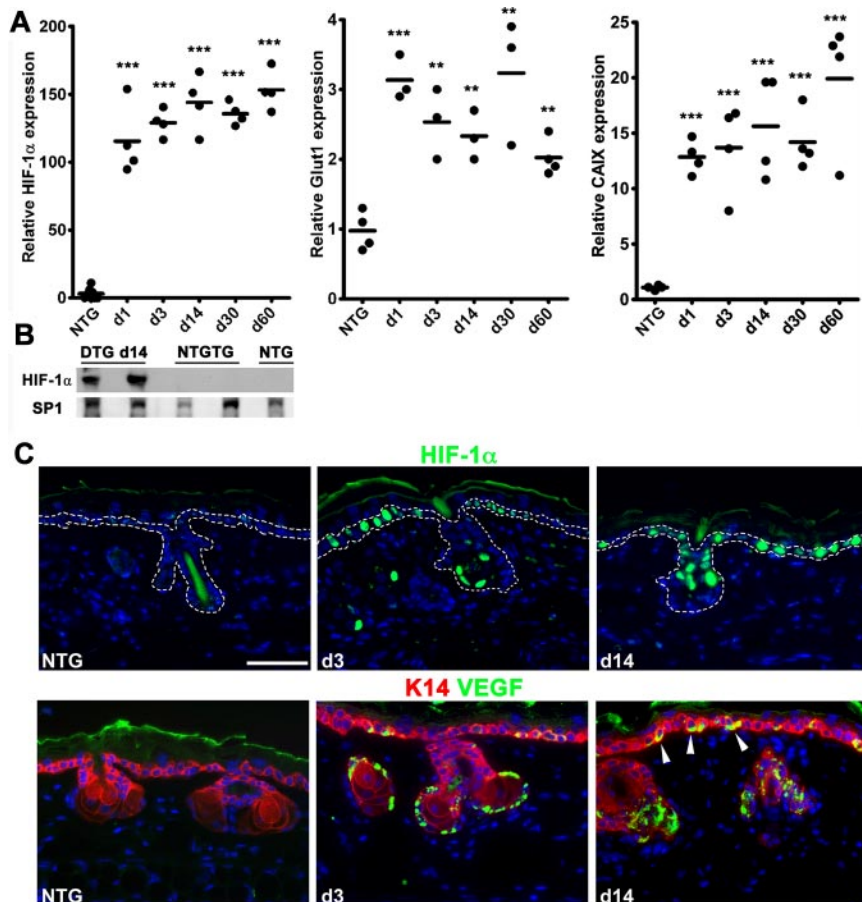


Figure 1. DOX HIF-1 α ^{P402A/P564A/N803A} transgene induction and target gene up-regulation. (A) Real-time reverse-transcribed polymerase chain reaction analysis of rapid and sustained elevations of transgene and "canonical" HIF-1 target gene mRNAs represented by glucose transporter-1 (Glut1) and CAIX in TetON-HIF-1 transgenic (denoted as "DTG" double transgenic) compared with NTG mice during continuous DOX induction. Prior analysis demonstrated no difference between NTG and DOX day 0 TetON-HIF-1 controls. (B) Transgene protein expression from Western blots of ear nuclear extracts on DOX day 14 in DTG, single TRE-HIF-1 α ^{P402/P464A/N803A} transgenic mice (NTGTG), or NTG controls. Each dot in scatter plots represents one mouse. Horizontal bars represent the mean. Gene expression measurements for HIF-1 α , Glut1, and CAIX were from the same samples. DTG data at each DOX day were compared with NTG or TetON-HIF-1 day 0 data (data not shown), using unpaired Student *t* test: ***P* < .01; ****P* < .001. (C) Representative HIF-1 α transgene and dual VEGF-keratin-14 immunofluorescence, showing expression localization in the interfollicular and hair follicle basal cell compartment after 3 and 14 days of DOX induction. Arrowheads indicate the basolateral VEGF localization within the basal cells. Bar represents 50 μ m.

killed by intracardiac paraformaldehyde perfusion, and ears collected for cross-sectional or whole-mount analysis.

AMD3100 treatment

TetON-HIF-1 mice were treated twice daily with AMD3100 (A 5602; Sigma-Aldrich), 1.25 mg/kg, or PBS intraperitoneally for 2 weeks.¹³ Mice were treated while on DOX for either days 0 to 14 or days 14 to 28, killed by intracardiac perfusion, and the ears analyzed for microvascular density and myeloid cell subsets by immunofluorescence.

Bone marrow cell isolation and transplantation

Recipient age-matched TetON-HIF-1 and NTG mice were irradiated with a single dose of 1000 cGy and bone marrow transplantations performed according to established protocols.¹⁷ Details are provided in supplemental Methods.

In vivo noninvasive label-free L-PAM

For longitudinal photoacoustic microscopy (L-PAM) of individual mice, 1 day before the experiment, the mouse ear was gently depilated (Surgi Cream; 82565; American International Industries). All mice received depilation, including both NTG and DOX day 0 mice. The lack of longitudinal changes in DOX-treated NTG mice from days 0 to 60 ruled out depilatory effects on the ear vasculature. At each time point (days 0, 1, 3, 14, 30, and 60), mice were anesthetized with 87 mg/kg ketamine and 13 mg/kg xylazine intraperitoneally, and transferred to a homemade stereotactic stage. Throughout the experiment, anesthesia was maintained using 1.0% to 1.5% isoflurane with an airflow rate of 1 L/min, and the body temperature of the animal was maintained at 37°C with a temperature-controlled heating pad. At the end of the longitudinal study, mice were killed by pentobarbital, 100 mg/kg, intraperitoneally. A schematic of the L-PAM system is presented in supplemental Figure 2A. Details of L-PAM design and analytical techniques, including segmentation analy-

sis of arteriovenous and capillary volumes, are provided in Supplemental data.¹⁸

Statistical analysis

Statistical analyses were performed using unpaired 2-tailed Student *t* tests comparing DOX-treated TetON-HIF-1 mice with either TetON-HIF-1 DOX day 0 or NTG mice using GraphPad Prism, Version 5 software. One-way analysis of variance was performed for comparisons between time points within DOX-induced TetON-HIF-1 mice treated with AMD3100. There were 4 to 10 mice per group unless indicated otherwise. The data are presented as scatter plots: each dot represents one mouse; and the horizontal bar indicates the mean. When bar graphs were used, the data represent the mean \pm SD, except as otherwise stated. All experiments were repeated a minimum of 2 times.

Results

Model development, transgene, and target gene expression kinetics

Basal keratinocytes were chosen as targets for conditional HIF-1 induction in TetON-HIF-1 double transgenic mice ("Mouse procedures") because they are epithelial cells distributed along the epidermal basement membrane, ideally positioned for paracrine signaling to the stroma.¹⁹ Ear skin was chosen for detailed investigation because of its paucity of fur and its frequent use in several transgenic and adenoviral-mediated angiogenesis studies.^{1,11,20,21} However, TetON-HIF-1 truncal skin displayed similar stromal alterations (data not shown). To control for purported antiangiogenic and protease inhibitor activities of DOX,²² NTG

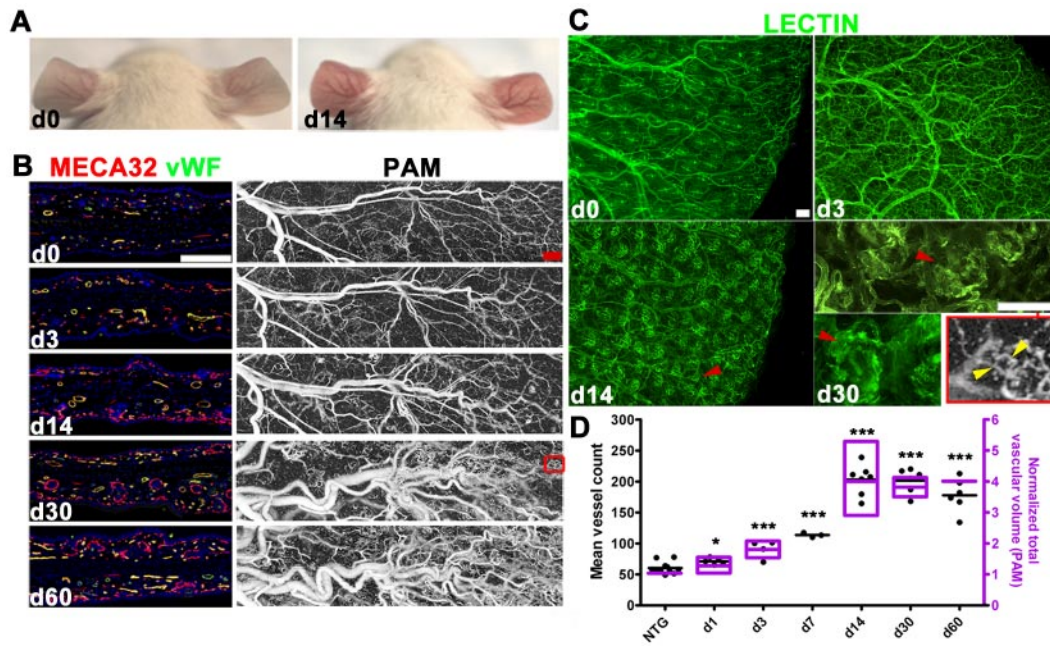


Figure 2. Multistage angiogenesis, microvascular network patterning, and serial noninvasive imaging of neovascularization by L-PAM in TetON-HIF-1 α transgenic mice. (A) Neovascular phenotype of a TetON-HIF-1 transgenic mouse with skin redness and vascular prominence developing 14 days after continuous DOX provision. (B) Comparative determination of TetON-HIF-1 neovascularization using immunofluorescent thin section microvessel markers, MECA32/vWF, with L-PAM. L-PAM was performed in the same transgenic mouse serially imaged for 60 days (red box represents the microvascular domain magnified in panel C). (C) Ear whole-mount images of FITC-*L. esculentum*-perfused TetON-HIF-1 mice over time (red arrowheads in day 14 and day 30 images indicate neocapillaries surrounding each rTA/HIF-1-expressing hair follicle). The L-PAM image insert (in grayscale) and the day 30 high-power whole-mount micrograph show similar conformation of the perifollicular neocapillaries. The yellow arrowheads indicate the vascular supply of the hair follicle capillary network. (D) Microvascular density as determined by vessel counting of MECA32/vWF double immunofluorescence tissue sections *ex vivo*, and microvessel volume derived from *in vivo* L-PAM of serially imaged individual TetON-HIF-1 mice ($n = 1-4$ for indicated time points) normalized to NTG controls, demonstrating the same trend of rapid elevation and then plateau by day 14. Data for each DOX day were compared with NTG or TetON-HIF-1 day 0 data (data not shown), using unpaired Student *t* test: * $P < .05$; ** $P < .01$; *** $P < .001$. Bars represent 200 μm (B) and 100 μm (C).

mice were fed DOX for intervals matching TetON-HIF-1 mice. As DOX day 0 TetON-HIF1 and NTG mice were phenotypically, microscopically, and molecularly similar, either genotype was used as a control in appropriate experiments. Transgene mRNA was up-regulated within 24 hours of DOX provision and remained elevated during continuous induction (Figure 1A). DOX-regulated transgene expression was slightly leaky at the mRNA level (data not shown) but tight at the protein level (Figure 1B). The mRNAs of 2 canonical HIF-1 target genes, GLUT1 and carbonic anhydrase IX, were rapidly induced and persistently elevated during continuous DOX exposure (Figure 1A). Further analysis demonstrated targeted HIF-1 α expression to interfollicular and hair follicle outer root sheath basal keratinocytes (Figure 1C; dashed line denotes basal keratinocyte compartment). VEGF was also expressed in the same epidermal basal keratinocyte cellular compartment (Figure 1C). The basolateral VEGF localization of keratinocyte VEGF (Figure 1C arrowheads) was particularly compelling, as it directly abutted the epidermal basement membrane immediately above the stromal region occupied by neovessels (see the next section). The stochastic expression pattern of HIF and VEGF was consistent with the original work describing K5-rtTA-regulated conditional epidermal transgene expression in adult mice.¹⁴ Further studies will need to be done to determine the mechanism for the difference between this stochastic transgene and target gene expression pattern and the near-uniform distribution of the neovasculature (see the next section).

Epithelial HIF-1 activation produces angiogenesis and a patterned microvasculature

DOX-induced TetON-HIF-1 mice developed skin redness and vascular prominence, noticeable on day 3 of continuous DOX

induction and peaking by DOX day 14 (Figure 2A). Histopathology was confined to the stroma, which displayed an increase in microvessels and mononuclear cells (data not shown). Vascular density increased 4-fold by day 14 (Figure 2B,D) with microvessels decorating the undersurface of the interfollicular epidermis and the hair follicles (Figure 2B). Whole mounts revealed development of a patterned neovasculature surrounding each hair follicle (Figure 2C). This microvessel organization was produced by keratin-5-regulated rTA induction in hair follicle outer root sheath cells and sebaceous glands that coordinately express keratin-14 (supplemental Figure 1A) as well as keratin-5 (data not shown).^{14,19} Endothelial tip cells with filopodia extending toward the transgene expressing epidermal cells were also detectable on day 3 of continuous DOX induction (supplemental Figure 1B).

Noninvasive determination of microhemodynamics during neovascularization

Label-free noninvasive L-PAM (supplemental Figure 2A-B) monitoring of individual DOX-induced TetON-HIF-1 transgenic mice from day 0 to day 60 demonstrated a progressive 4-fold elevation in total microvessel volume, concordant with immunofluorescent vessel density analysis (Figure 2B,D; supplemental Figure 2E). L-PAM also resolved the perifollicular neovascular capillaries, as well as microvessels supplying the capillary plexus (Figure 2C, yellow arrowheads in the red boxed L-PAM close-up). Two-dimensional projection images (Figure 2B) and 3-dimensional rendering (supplemental Video 1) further revealed extensive dilatation, tortuosity, and remodeling of large-caliber arteriovenous

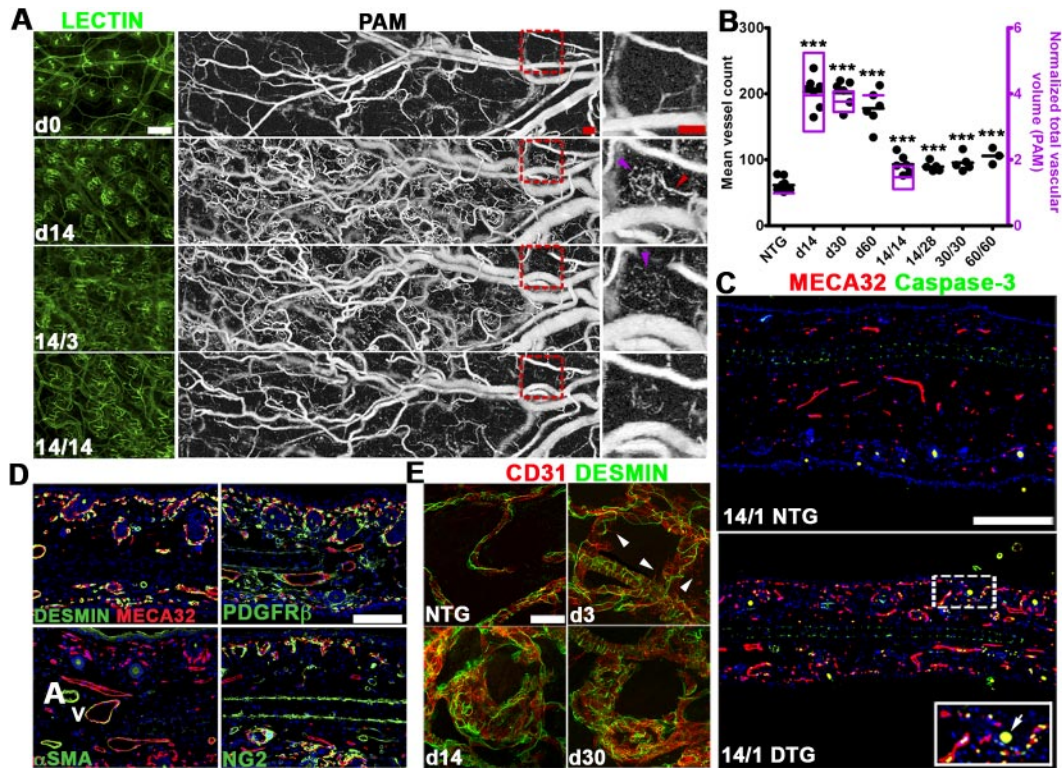


Figure 3. Pericyte marker expression and microvessel stability after HIF-1 withdrawal. (A) Representative lectin-perfused whole mounts (left column) and L-PAM images (middle and right columns) during HIF-1 induction (day 0, day 14) followed by DOX withdrawal 14/3 (14 days ON/3 days OFF), 14/14 (14 days ON/14 days OFF). Neocapillaries that developed farthest from the hair follicles remain after withdrawal accounting for a persistent 30% increase in vascularity compared with DOX day 0 or NTG controls. L-PAM images are obtained from the same TetON-HIF1 transgenic mouse imaged over 28 days. L-PAM detects development of a perifollicular neocapillary unit (purple arrowhead) with its adjacent vascular supply arch (red arrowhead), capillary luminal diminution with “single file” RBCs on withdrawal day 3 (purple arrowhead), and involution with persistence of peripheral microvessels by withdrawal day 14 (right column). (B) Quantification of microvessel density (MECA32 immunofluorescence, in black) and volume (L-PAM, in purple) in TetON-HIF-1 on DOX day 14, day 30, and day 60, and after increasing intervals of DOX activation followed by commensurate periods of withdrawal, 14/14, 14/28, 30/30, and 60/60 (n = 1-5). (C) Induction of endothelial cell apoptosis (dual-positive, MECA32/caspase-3 cells, arrowheads right panel) subjacent to epithelial basal cell compartments of the hair follicle and interfollicular epidermis (dashed dotted square and enlarged inset, white arrow denotes the hair shaft) after one day of DOX withdrawal (lower panel). (D) Thin section dual-endothelial (MECA32) and pericyte marker immunofluorescence demonstrates coverage of TetON-HIF-1 DOX day 14 induced microvessels by desmin, PDGFR β , and NG2. α -SMA expression was restricted to arteries (A) and veins (V) as delineated morphologically and by the SMA expression pattern. (E) Confocal immunofluorescence demonstrates extensive and intimate microvessel coverage by desmin-positive pericytes at all time points after DOX induction (arrowheads delineate endothelial tip cells also shown in detail in supplemental Figure 1B). TetON-HIF-1 data at each DOX day were compared with NTG or TetON-HIF-1 day 0 data (data not shown), using unpaired Student t test: * $P < .05$; *** $P < .001$. Bars represent 100 μ m (A,D), 200 μ m (C), and 20 μ m (E).

vessels during continuous epithelial HIF-1 activation (supplemental Figure 2D,F-G). Using L-PAM’s resolution and depth-sectioning capability, we determined the kinetics of capillary versus arteriovenous volume changes for extended intervals after HIF-1 induction, based on vessel caliber and 3-dimensional morphology^{18,23} (supplemental Figure 2D-E; supplemental Methods). Capillary volume tripled on day 3 and then abruptly increased to a 15-fold elevation by day 14 predominantly because of capillary genesis. Capillary volume remained at the same elevated level from day 14 to day 60. In contrast, arteriovenous vessel volume expansion was more gradual, modest, and persistent, reaching a 3- to 4-fold elevation by day 60. Arteries and veins also evidenced increased tortuosity, defined as the ratio of the vessel length to the linear distance between 2 adjacent bifurcation points, between day 14 and day 60 (Figure 2B; supplemental Figure 2D,F-G). The volume increase for the entire neovasculature was similar to that of the arteriovenous network, which composed the majority of total vessel volume (supplemental Figure 2E). NTG mice treated with DOX from day 0 to day 60 evidenced no change in vessel density or volume either by L-PAM or immunofluorescence (supplemental Figure 2C,E-F). Collectively, these L-PAM and vascular density data demonstrate that TetON-HIF-1 neovascularization is composed of 2 stages after DOX-HIF-1 induction: a development stage consisting of angiogenesis, microvessel growth, and organization

into perifollicular microvascular clusters, and a maintenance stage wherein the capillary network is metastable (see the next section) and the arteriovenous vessels continuously remodeled.

Dynamics of microvascular regression after transgene withdrawal, independent of endothelial pericyte coverage

Temporal HIF-1 control allowed us to determine mechanisms of microvascular stability or regression after transgene and consequent angiogenic factor withdrawal. HIF-1 was DOX-induced for 14, 30, or 60 days to produce a neovasculature and then withdrawn for increasing intervals ranging from 1 to 60 days (Figure 3A-B). Microvessel persistence was exquisitely dependent on continuous epithelial HIF-1 function, with a 2-fold overall reduction of vascular density on DOX withdrawal (Figure 3B). Whole mounts demonstrated a marked dropout of perifollicular microvessels as early as postwithdrawal day 3, with persistence of neovessels that developed at the greatest distance from the transgene expressing hair follicles (supplemental Figure 3A). Overall, there was a permanent 30% microvessel increment compared with controls (Figure 3A-B; supplemental Figure 3A). Longer periods of transgene expression, either for 30 or 60 days, did not produce further increases in permanent neovessels (Figure 3B). Endothelial and perivascular cell apoptosis was activated as early as day 1, peaked

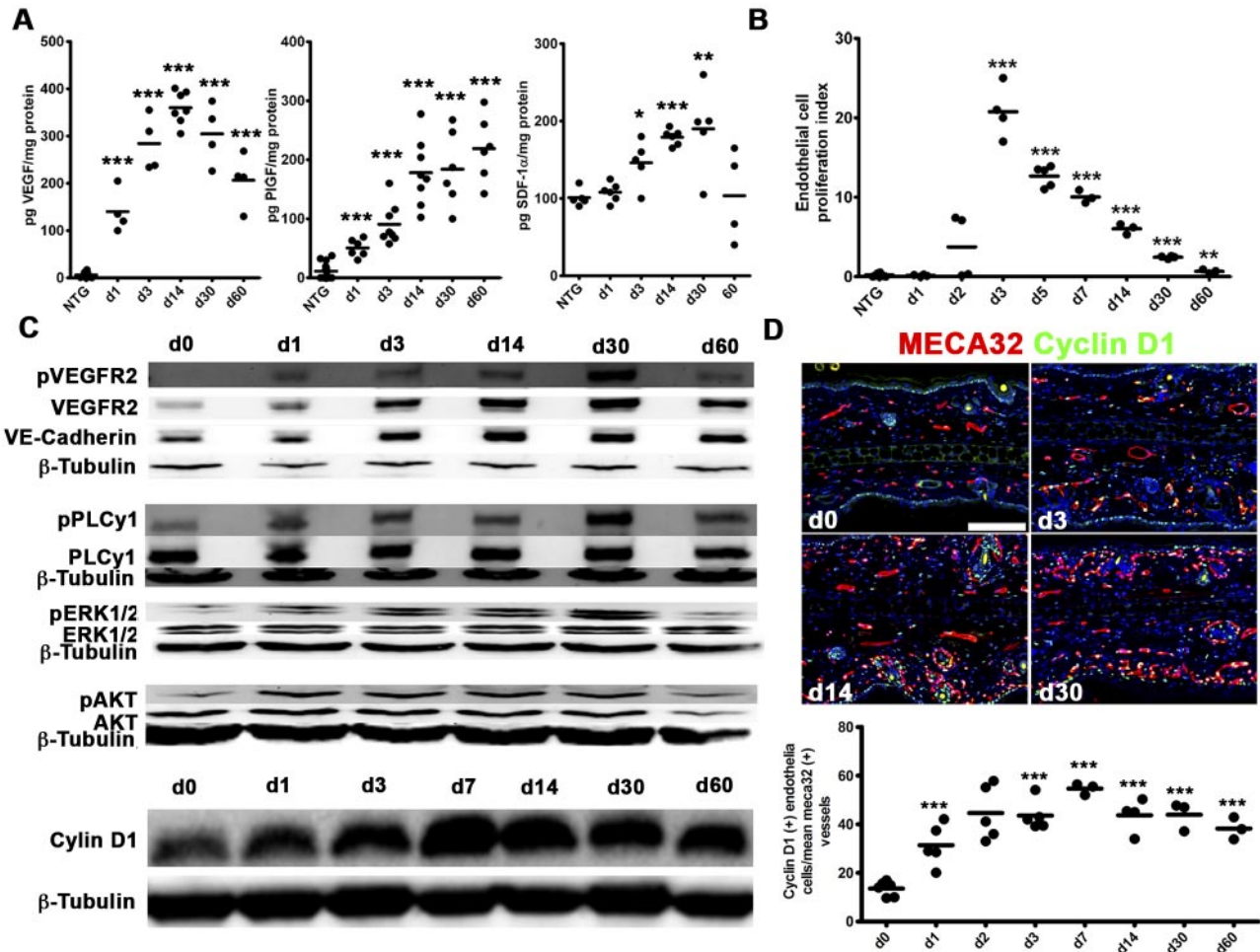


Figure 4. Up-regulation of HIF-1 angiogenic factor transcriptional targets, persistent VEGFR2 signaling, and intrinsic down-regulation of endothelial proliferation in TetON-HIF-1 transgenic mice. (A) Ear tissue ELISA for VEGF (left), PlGF (middle), and SDF-1 (right). Immediate day 1 increase of VEGF and PlGF contrasts the gradual SDF-1 induction between day 3 and day 30. (B) TetON-HIF-1 endothelial cell proliferation kinetics determined by counting double-labeled 5-bromo-2'-deoxyuridine/MECA32-positive endothelial cells in four to six $10\times$ fields per thin section normalized to the microvascular density. (C) Representative Western blot analysis of total ear tissue lysates for VE-cadherin, total and phosphorylated: VEGFR2^(Y1173), PLC γ ^(Y783), ERK1/2^(T202/Y204), AKT^(S473), and cyclin D1. (D) Representative immunofluorescent images (top) and quantification (bottom) of cyclin D1. TetON-HIF-1 data at each DOX day were compared with NTG or TetON-HIF-1 day 0 data (data not shown), using unpaired Student *t* test: **P* < .05; ***P* < .01; ****P* < .001. Bar represents 100 μ m.

on day 3, and fell to near-baseline levels by withdrawal day 14 (Figure 3C; supplemental Figure 3D). Apoptotic endothelial cells were most frequently detected immediately adjacent to the formerly transgene-expressing hair follicle and interfollicular basal cells (Figure 3C, dotted white square and inset enlargement), suggesting that these microvessels were “addicted” to high angiogenic factor levels. DOX withdrawal experiments defined the third stage of TetON-HIF-1 neovascularization, HIF-1–dependent microvessel regression.

The high resolution and large field of view of L-PAM functionally delineated the entire process of neovascular regression (Figure 3A middle column). Magnified images showed a preexisting microvascular feeder loop on day 0 and perfollicular neovessel establishment by day 14 with feeder loop dilatation (Figure 3A right column, red and purple arrowheads). On withdrawal day 3, these neovessels were intact, though of markedly decreased luminal diameter, as individual red blood cells (RBCs) with intervening gaps, probably plasma, were delineated by L-PAM (Figure 3A purple arrowhead; each white dot represents a single RBC). By withdrawal day 14, most of these neovessels regressed with persistence of the peripheral capillary ring.

As pericytes can convey microvascular stability, we predicted that they would be sporadically or loosely associated with TetON-HIF-1 capillary endothelial cells, given the marked microvessel transgene dependence (see “Epithelial HIF-1 activation up-regulates angiogenic target genes and produces persistent VEGFR2 signaling discordant with endothelial proliferative quiescence”), and the multiple potential angiogenic HIF-1 target genes.²⁴ Moreover, we also predicted that endothelial pericyte coverage would be lacking or sparse on development stage microvessels, as previously reported in studies of postnatal retinal vascular development.²⁵ However, neither prediction was correct in TetON-HIF-1 mice. Desmin-positive pericytes tightly covered each microvessel throughout neovascular development and maintenance, from day 0 to day 30, including vessels closest to high-level multiangiogenic growth factor expression, the perfollicular and subepidermal microvasculature (Figure 3D-E; supplemental Figure 3B). We also delineated dynamic alterations in pericyte marker expression. Although desmin was constitutively present in perivascular cells, PDGFR β and NG2 expression was undetectable during DOX days 1 to 3, then up-regulated by day 14, but again undetectable by DOX day 30 (supplemental

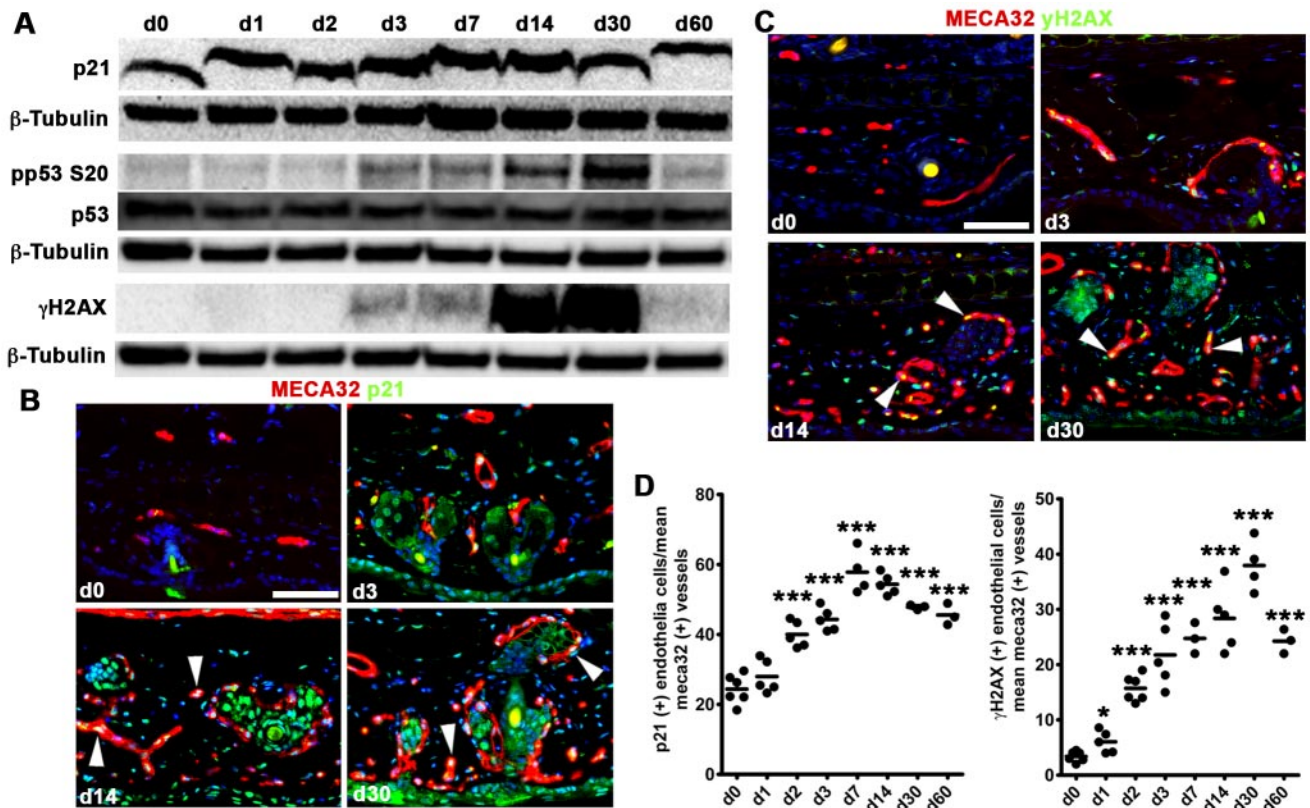


Figure 5. Activation of epithelial HIF-1 induces a DNA damage/replication stress checkpoint. (A) Western analysis of p21, total and phosphorylated p53^{S20}, and phosphorylated γ -H2AX reveals induction of cell-cycle inhibitors consistent with replication stress beginning at peak endothelial proliferation (Figure 4). (B-C) Representative thin ear tissue immunofluorescent images of p21 (B) and γ -H2AX (C). White arrowheads point to p21 and γ -H2AX–positive endothelial cells. (D) Quantification of p21 and γ -H2AX expression determined by vessel counting of MECA32/p21 and MECA32/ γ -H2AX double immunofluorescence tissue sections ex vivo. TetON-HIF-1 data at each DOX day were compared with TetON-HIF-1 day 0 data, using unpaired Student *t* test: **P* < .05; ***P* < .01; ****P* < .001. Bar represents 50 μ m.

Figure 3B). α -Smooth muscle actin (α -SMA) expression was restricted to large-caliber stromal arteries and veins that were defined by shape and staining pattern (Figure 3D). In particular, arteries were oval or ovoid with thick walls and continuous high-level SMA staining, whereas veins were enlarged, irregular ellipsoids with discontinuous, low-level SMA expression (Figure 3D; supplemental Figure 3C). α -SMA staining also further highlighted the fact that SMA-negative capillaries were the predominant microvessel subset engaged in HIF-1–dependent population expansion (Figure 1B) during DOX induction and in apoptosis after DOX withdrawal (Figure 3C). These data reveal that the type of pericyte marker expressed on neovessels is temporally regulated, and in addition, controlled by the microvessel tissue and biologic context.²⁶

Epithelial HIF-1 activation up-regulates angiogenic target genes and produces persistent VEGFR2 signaling discordant with endothelial proliferative quiescence

To probe the molecular underpinnings of epithelial HIF-1-mediated neovascularization and regression, we determined DOX-induced alterations of angiogenic HIF-1 target genes (supplemental Figure 4A-C). VEGF, PIGF, PDGF-B, and iNOS mRNAs rapidly increased and then plateaued or decreased. Adrenomedullin, SDF-1 α , and angiopoietin-2 slowly rose, whereas thrombospondin-1, an angiogenesis inhibitor and a target of suppression by hypoxia,²⁷ progressively decreased. VEGF and PIGF protein were both persistently up-regulated 20- to 60-fold and 4- to 20-fold, respec-

tively (Figure 4A), with a comparatively modest 1.9-fold SDF-1 α peak induction.

Continuous angiogenic growth factor expression led us to determine endothelial proliferation kinetics. Initiation of endothelial proliferation required 24 hours of transgene activation (Figure 4B; supplemental Figure 4D). Proliferation peaked on day 3 but exponentially decreased thereafter (Figure 4B). Endothelial proliferation was also detectable in microvessels morphologically classified as arterioles and venules (supplemental Figure 4D, “A” and “V” labels). As prolonged endothelial cell VEGF stimulation can produce divergent effects on VEGFR2 protein expression, either down-regulation^{28,29} or induction and maintenance,³⁰ we hypothesized that diminution of receptor expression or activation would be associated with cessation of proliferation in TetON-HIF-1 endothelium. However, whole tissue levels of both total and phosphorylated (Y¹¹⁷³) VEGFR2 in DOX day 0 to day 60 TetON-HIF-1 ears were persistently elevated 6- to 10-fold compared with controls (Figure 4C; supplemental Figure 5A). Fluorescence microscopy demonstrated persistent endothelial VEGFR2 expression and receptor up-regulation in perifollicular and subepidermal endothelial cells (supplemental Figure 5B). The major VEGFR2 signaling outputs (ie, AKT, PLC- γ , and ERK phosphorylation) each persistently increased 2- to 6-fold, from day 1 to day 30 (Figure 4C; supplemental Figure 5A). Cyclin D1 was also persistently up-regulated 2- to 6-fold after transgene induction (Figure 4C; supplemental Figure 5A). Immunofluorescence localized cyclin D1 expression to TetON-HIF-1 endothelial cell nuclei (Figure

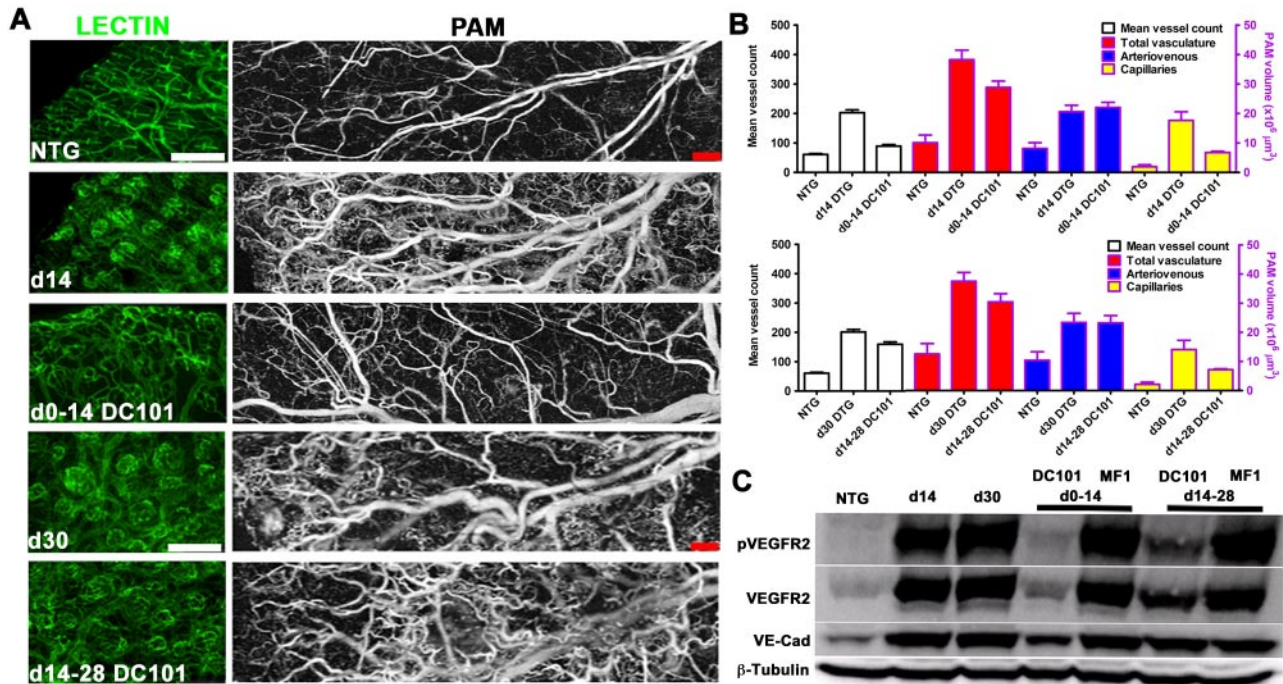


Figure 6. Stage-specific resistance of the HIF-1 neovasculature to VEGFR1 and VEGFR2 immuno-blockade. (A) Inhibition of the development (days 0-14) versus resistance of the maintenance stage (days 14-28) to VEGFR2 (DC101) immuno-blockade as determined by lectin whole-mount and L-PAM analysis. Both L-PAM and FITC-*L. esculentum*-perfused whole mounts demonstrate the marked sensitivity of perifollicular neocapillaries, whereas microvessels farthest from HIF-1 production are resistant to DC101. L-PAM also detected arteriolar and venular dilatation resistant to DC101 treatment in both stages. (B) Quantification of diminution of microvessel density by cross-sectional MECA32-VWF immunofluorescence (white bars; immunofluorescence data not shown) or volume reduction delineated by image extraction L-PAM analysis during day 0 to day 14 (top) or day 14 to day 28 (bottom) VEGFR2 blockade (blue and yellow bars). (C) Western blot analysis of vascular endothelial-cadherin (VE-Cad), VEGFR2^{Y1173}, and total VEGFR2 in mice treated with VEGFR1/2 blocking antibodies. Bars represent 200 μm .

4D). Thus, neither down-regulation of VEGFR2 expression, activation, and signaling outputs, nor persistent G1 activation was responsible for the temporally regulated, intrinsic endothelial cell proliferative resistance in the context of continuous angiogenic growth factor stimulation.

To further probe mechanisms of endothelial proliferation down-regulation, we determined the kinetics of cell-cycle repressors in TetON-HIF-1 tissue extracts. Activated phospho-p53^{S20} was elevated 3-fold coincident with day 3 peak endothelial proliferation, and remained 3- to 7-fold increased to day 30 (Figure 5A; supplemental Figure 6A). The p53 target p21 was also induced 4-fold at peak endothelial proliferation and remained persistently elevated (Figure 5A; supplemental Figure 6A). Immunofluorescence revealed p21 induction and persistence in endothelial cell nuclei (Figure 5B white arrowheads; Figure 5D). As these data suggested replication stress as a mechanism for cell-cycle inhibition, we probed tissue extracts for activation of the stress/DNA damage mediator γ -histone H2AX (γ -H2AX). γ -H2AX was induced 50-fold by day 3 with further increases in protein expression between day 14 and day 30. Expression at day 60 remained 16-fold elevated compared with day 0 (Figure 5A; supplemental Figure 6A). Immunofluorescence also revealed endothelial cell nuclear γ -H2AX induction (Figure 5C white arrowheads). Quantitative analysis delineated a 5-fold elevation of γ -H2AX-positive endothelial cell nuclei by day 3 and sustained at that level thereafter (Figure 5D). Further analysis of the day 0 and day 3 time points using confocal microscopy identified endothelial cells containing multiple γ -H2AX-positive nuclear foci (supplemental Figure 6B; and data not shown).

Stage-specific differential responsiveness to VEGFR1/2 inhibitors

TetON-HIF-1 multistage angiogenesis was a unique platform to temporally dissect the functional contributions of VEGFR2 or VEGFR1 signaling to neovascularization. Day 0 to day 14 VEGFR2 immuno-blockade with DC101³¹ produced a 2.3-fold reduction in microvessel density primarily because of inhibition of perifollicular neovessel formation (Figures 6A-B, 7A; supplemental Movie II). Western blotting revealed a 10-fold diminution of VEGFR2 phosphorylation in this same interval (Figure 6C; and data not shown). In vivo noninvasive L-PAM image extraction analysis detected a 2.9-fold diminution in capillary volume that nearly matched microvessel counting of tissue sections, whereas elevated arteriovenous and total vessel volumes were unaffected (Figure 6B). VEGFR1 blockade by MF1³² did not affect day 0 to day 14 microvessel density (Figure 7A), whereas a DC101/MF-1 cocktail was similar to single-agent DC101 (data not shown).

In contrast to day 0 to day 14, there was resistance of the TetON-HIF-1 microvasculature to either single-agent DC101 or DC101/MF-1 cocktail deployment between day 14 and day 28 that was also evident in the L-PAM datasets (Figures 6A-B, 7A; supplemental Video 2). Microvessel density was reduced by only 20% compared with DTG day 30 (Figure 6B left-most bar graph). Western analysis also mirrored resistance with a 2.5-fold reduction in phospho-VEGFR2 (Figure 6C). L-PAM microvessel subset extraction analysis revealed only a 1.9-fold reduction in capillary and essentially unchanged arteriovenous volumes during VEGFR2 (Figure 6B) or combinatorial VEGFR1/2 blockade (data not shown). MF1 increased microvascular density by 30% during day

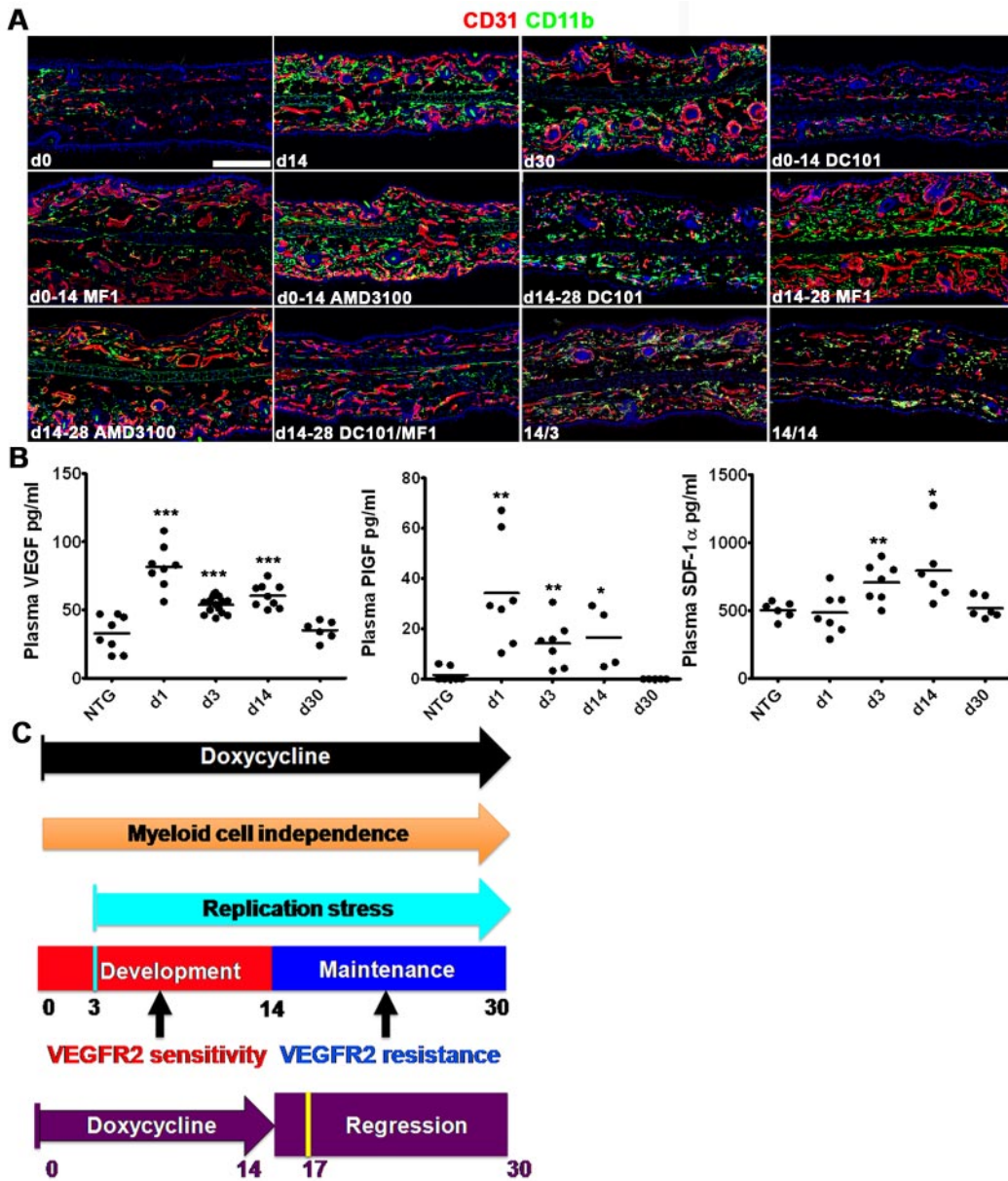


Figure 7. Stage-specific regulation of stromal myeloid cell recruitment and retention. (A) Representative CD31/CD11b coimmunofluorescence demonstrating recruitment and stromal accumulation of CD11b myeloid cells during the TetON-HIF-1 DOX day 0 to day 14 neovascular development stage, with HIF-1–dependent retention of these cells from day 14 to day 28. Myeloid cell recruitment is markedly inhibited by VEGFR1 (MF1) or VEGFR2 (DC101). Notably, neovascular development proceeds despite marked inhibition of myeloid cell recruitment in MF1-treated TetON-HIF-1 mice. AMD3100 partially inhibits myeloid cell recruitment (supplemental Figure 8B). DOX day 14 to day 28 myeloid cell retention is independent of either VEGFR1 or VEGFR2 but dependent on signaling from both receptors. Myeloid cell retention is incompletely inhibited by AMD3100 (supplemental Figure 8). The maintenance stage neovasculature persists despite profound stromal myeloid depletion in the day 14 to day 28 DC101/MF1 inhibitor cocktail-treated TetON-HIF-1 mice. Stromal myeloid cells rapidly disappear after 3 (14/3) and 14 (14/14) days of DOX withdrawal. (B) Plasma VEGF (left), PIGF (middle), and SDF-1 α (right) expression levels in TetON-HIF-1 mice and DOX NTG controls determined by ELISA. TetON-HIF-1 data at each DOX day were compared with NTG or TetON-HIF-1 day 0 data (data not shown), using unpaired Student *t* test: **P* < .05; ***P* < .01; ****P* < .001. (C) Model of epithelial neovascularization regulated by HIF-1. Continuous HIF-1 activation produces multistage intrinsically regulated neovascular development, maintenance, and transgene-dependent regression. Mechanisms of myeloid cell recruitment and retention were stage-specific. Resistance to VEGFR2 immuno-blockade was also stage-specific. The cyan bar represents peak proliferation achieved at day 3; dark orange arrow, neovascular growth and maintenance independent of myeloid cells; purple arrow, 14 days of continuous DOX induction; purple bar, 14 days of DOX withdrawal; yellow bar, peak apoptosis and L-PAM–determined capillary luminal constriction 3 days after DOX withdrawal. TetON-HIF-1 data at each DOX day were compared with NTG data, using unpaired Student *t* test: **P* < .05; ***P* < .01; ****P* < .001. Bar represents 200 μ m.

14 to day 28 (Figure 7A; and data not shown), consistent with VEGFR1 function as VEGF “sink” on endothelial cells.

Stage-specific myeloid cell inhibitor responsiveness and dissociation of myeloid cells from neovascular development or maintenance

As myeloid cells enhance tumor or ischemic angiogenesis³³ and contribute to angiogenic inhibitor evasion,³⁴ we tested for their

recruitment and retention from day 0 to day 30 of HIF-1 activation. CD45, CD11b myeloid cells, mast cells, and F4/80 macrophages were progressively recruited to the stroma during the TetON-HIF-1 day 0 to day 14 development stage and were retained during the day 14 to day 30 maintenance stage (Figure 7A; supplemental Figures 7A-B, 8A). Neutrophils were also recruited and retained during these stages, though to a lesser extent than CD11b cells or F4/80 macrophages (supplemental Figure 7C). Myeloid cell retention

required continuous epithelial HIF-1 expression, as they rapidly disappeared from the stroma after 3 days, and returned to baseline levels by 14 days of DOX withdrawal (Figure 7A). A bone marrow origin for the recruited myeloid cells was suggested by autologous bone marrow transplantation using CAG-EGFP donor cells (supplemental Figure 7D).

To determine mechanisms of myeloid cell recruitment and retention, we first tested for endocrine angiogenic growth factor secretion from DOX-activated skin. There was a rapid 2.5- and 15-fold elevation of plasma VEGF and PlGF, respectively, on DOX day 1, both falling to control levels by day 30 (Figure 7B). In contrast, plasma SDF-1 was only 1.4- to 1.5-fold elevated on day 3 and day 14, returning to baseline by day 30 (Figure 7B right panel). Transient elevation of these angiogenic growth factors in plasma contrasted with their continual high-level expression in tissue (Figure 4A; supplemental Figure 4A-C). As previous work demonstrated the principal involvement of the VEGF/PlGF/VEGFR1 signaling module in recruitment,³⁵ and SDF-1/CXCR4 engagement in retention,^{2,36} we tested inhibitors of these signaling axes in both the development and the maintenance stages. As expected, either MF1-mediated VEGFR1 or DC101-mediated VEGFR2 immuno-blockade abrogated myeloid cell recruitment during the development stage (Figure 7A). However, the presence of robust neovascularization in the absence of stromal myeloid cells revealed by VEGFR1 blockade was unexpected (Figure 7A). Whereas CXCR4 blockade by AMD3100 did not alter development stage neovascularization, it decreased CD11b myeloid cell recruitment by 31% compared with nontreated DTG mice (Figure 7A; supplemental Figure 8B). Whereas maintenance stage myeloid cell retention was unaffected by either single-agent DC101 or MF-1, it was nearly abrogated by a DC101/MF1 “cocktail” (Figure 7A; supplemental Figure 8C). Potent inhibition of myeloid cell retention again revealed a striking disconnection between loss of stromal myeloid cells and persistence of the HIF-1 neovasculature. AMD3100, used at doses previously shown to decrease tumor and VEGF-mediated myeloid cell retention and hypervascularization,^{2,13} failed to affect maintenance stage microvascular density but did produce a 54% decrease myeloid cell retention (Figure 7A; supplemental Figure 8A). In contrast to HIF-1 α and VEGF, SDF-1 α was more uniformly expressed in basal transgenic keratinocytes (supplemental Figure 8C). However, in contrast to previous work, this chemokine was rarely detectable in perivascular² and endothelial cells.³⁶

Discussion

Here, using detailed kinetic analysis, we discovered that neovascular development was intrinsically regulated by a DNA damage checkpoint in endothelial cells coincident with peak endothelial proliferation. Each neovascular stage also possessed distinctive vascular and myeloid cell responses to angiogenesis inhibitors (Figure 8). TetON-HIF-1 mice enabled development of L-PAM, which noninvasively and without intravenous contrast, mapped neovascular network architecture and vessel volumetric changes during emergence, maintenance, regression, or angiogenesis inhibitor responsiveness.

Cell autonomous inhibition of TetON-HIF-1 endothelial cell proliferation was surprising given the continuous microvessel exposure to elevated levels of angiogenic factors. Down-regulation of VEGFR2 expression levels and activation could have been responsible for diminution of proliferation; however, both immuno-

fluorescence and Western blotting analysis demonstrated persistent expression and microvessel localization. Persistent VEGFR2 expression and activation were unexpected because receptor tyrosine kinases as a class are down-regulated via internalization and degradation after growth factor activation.³⁷ However, VEGFR2 cell biology is complex, with contextual regulation of expression level, intracellular compartmentalization, and signaling.^{28,30,38} A more attractive mechanism for cell autonomous regulation of endothelial proliferation was induction of replication stress resulting from continuous endothelial cell stimulation by angiogenic growth factors, here predominantly VEGF.³⁹ Support for this hypothesis was based on several pieces of data, including persistent VEGFR2 expression and phosphorylation, continuous cyclin D1 up-regulation in endothelial cells, and induction and sustained expression of endothelial cell p21 and γ -H2AX. Localization of γ -H2AX to nuclear foci, consistent with DNA strand breaks, was also compelling data in support of replication stress.⁴⁰ Prior work demonstrated that γ -H2AX was required for neovascularization in ischemia and in growing tumors.⁴¹ However, that work suggested that γ -H2AX predominantly regulated endothelial proliferation during hypoxia. Here we demonstrated that replication stress and γ -H2AX were probably important for regulation of endothelial proliferation in normoxia and in response to continuous angiogenic factor stimulation. One possible mediator of endothelial cell replication stress is HIF-1 α . HIF-1 α can induce a DNA damage response, in the absence of hypoxia, because of inhibition of Nbs1, a crucial component of the MRN DNA repair complex.⁴² As HIF-1 is also a part of a VEGF-mediated autocrine signaling loop in endothelial cells,¹² MRN inhibition may be responsible for γ -H2AX induction in our model and will be investigated in future studies. Collectively, these studies and our data highlight the ability of conditional models of neovascularization to uncover endothelial cell regulation mechanisms that are independent of disease.

The endothelial-pericyte biology during epithelial HIF-1-mediated neovascularization was unanticipated. Lack of detectable “naked” endothelial tubes subsequently recruiting pericytes was contrary to studies of the neonatal rodent retina.^{25,43} However, coincident pericyte-endothelial envelopment during microvessel assembly and pericyte-mediated endothelial tip cell guidance during stromal invasion have both been reported.⁴⁴⁻⁴⁶ Intimate microvessel envelopment was also unexpected as HIF-1 created a tumor-like angiogenic growth factor milieu, which has been correlated with loose pericyte-endothelial association.⁴⁷ Most surprising was the dissociation of pericyte coverage, transgene-dependent neovascular regression, and VEGF inhibitor resistance. As such, pericytes and vessel “maturation” could have been evoked as an explanation for VEGFR2 inhibitor resistance. However, extensive pericyte coverage was insufficient to maintain the neovasculature after HIF-transgene withdrawal.

Stage-specific alteration of stromal myeloid cell recruitment and retention by VEGFR2 or VEGFR1 was also unanticipated. Prevention of stromal myeloid cell recruitment in the development stage by MF1 was consistent with known mobilization and chemotactic functions of VEGFR1 on hematopoietic precursors.⁴⁸ DC101's inhibition of day 0 to day 14 myeloid cell recruitment was consistent with an abrogation of both endothelial cell luminal receptor up-regulation and VEGF proinflammatory functions.²⁰ In contrast, maintenance stage myeloid cell retention was resistant to either MF1 or DC101 but exquisitely sensitive to dual VEGFR1/VEGFR2 immuno-blockade. Previous work demonstrated VEGFR2 expression on tumor infiltrating myeloid cells.⁴⁹ Our data now suggest a functional role for VEGFR2 expression in myeloid cell

retention that will need to be tested in disease models. Equally surprising was the minimal effect of CXCR4 blockade, particularly on myeloid cell retention. These results were in contrast with the potent ability of CXCR4 blockade to decrease both stromal myeloid cell retention and microvascular density in ischemia, tumor xenografts, and conditional VEGF induction models.^{2,13,36} Our study suggests that the SDF-1 signaling requirement for myeloid retention is cell context, tissue, and disease dependent. Most surprising was the persistence of the HIF-1 microvasculature during maintenance stage DC101/MF-1-mediated myeloid cell depletion, as these cells are the source of multiple angiogenic factors responsible for VEGF inhibitor evasion or amplification of therapeutic angiogenesis in preclinical tumor or ischemia models.^{13,36,50,51} As such, our work highlights the fact that myeloid cell accumulation in angiogenic tissues does not necessarily support neovascular persistence. Rather the bona fide ischemic or tumor microenvironment is required for proangiogenic myeloid cell subset production.

PAM, combining optical excitation and ultrasonic detection, has multiple attractive features. First, the endogenous hemoglobin absorption contrast enables PAM to identify RBC-perfused microvasculature, the functional vascular subset responsible for tissue oxygen supply.⁵² Second, the one-way ultrasonic path enhances tissue transparency because acoustic scattering in biologic tissues is much weaker (1000 times less) than optical scattering. Third, the combination of the high nonradiative quantum yield of hemoglobin, the perfect 100% sensitivity of PAM to optical absorption, and the enhanced tissue transparency enables imaging sensitivity down to the single RBC level with a low laser exposure (contrast-to-noise ratio is ~ 100:1 with 570-nm laser excitation).⁵³ Fourth, the combination of the contrast-free preparation and low-level laser exposure enables noninvasive repetitive imaging of chronic processes including, but not limited to, temporal angiogenesis. With the present L-PAM, we were able to dissect neovascular elaboration in TetON-HIF-1 mice at the capillary level in the same animal for prolonged observation intervals (60 days, or more if necessary). The feature extraction capability of L-PAM enabled determination of the differential responsiveness of capillaries versus arteriovenous vessels to angiogenic inhibitors. Emergent translational L-PAM advances are focusing on imaging and therapy monitoring for skin cancer, breast cancer, and internal yet endoscopically accessible organs, such as esophagus, colon, and bladder, in cancer patients.

In conclusion, the TetON-HIF-1 mouse model revealed novel aspects of neovascular regulation divergent from previous preclinical studies but strikingly convergent with clinical challenges, facing both angiogenesis inhibitors in cancer and vascular restora-

tion in ischemia. L-PAM's ability to both longitudinally image neovascularization and to segment microvessel subset responses to angiogenesis inhibitors will be a boon to the study of ischemic and tumor neovascularization.

Acknowledgments

The authors thank Rebecca Sohn for mouse husbandry; Rick Bruick for the gift of the TRE-HIF-1 α ^{P402A/P464A/N803A} plasmid for construction of the TRE-HIF-1 α ^{P402/464A/N803A} transgenic mice; Adam Glick for the gift of the K5-rtTA transgenic mice; ImClone for the generous gift of the DC101 and MF1 antibodies; Fulu Liu, Alyssa Gregory, Kyle Eash, and Dan Link for help with bone marrow transplantation and advice on AMD3100 experiments; and Professor James Ballard for reading the manuscript.

This work was supported by National Institutes of Health grants R01-CA90722, R01-EB000712, R01-NS46214, R01-EB008085, and U54-CA136398.

Authorship

Contribution: S.S.O. contributed to experimental design, coordinated the research project, performed most of the biology experiments, analyzed data, prepared figures, and wrote the manuscript; S.H. contributed to the experimental design, performed all L-PAM imaging and data analysis, prepared figures, and wrote the manuscript; A.C.S. performed ear whole-mount and confocal microscopy experiments and edited the manuscript; J.Y. performed L-PAM data analysis, assisted with L-PAM experiments, organized figures, and wrote the manuscript; J.R.K. performed the myeloid cell immunofluorescence experiments; R.V.S. provided the TRE-HIF-1 α ^{Pro402A/564A/Asn803A} mice and edited the manuscript; K.M. contributed to L-PAM technology development and the L-PAM experiments; L.V.W. conceived and designed L-PAM experiments and wrote the manuscript; and J.M.A. conceived, designed, and directed the overall research project, analyzed data, and wrote and edited the manuscript.

Conflict-of-interest disclosure: L.V.W. has financial interest in Microphotoacoustics Inc and Endra Inc, which, however, did not support this work. The other authors declare no competing financial interests.

Correspondence: Jeffrey M. Arbeit, 660 South Euclid Ave, Campus Box 8242, St Louis, MO 63110; e-mail: arbeitj@wustl.edu; or Lihong V. Wang, One Brookings Dr, Campus Box 1097, St Louis, MO 63130; e-mail: lhwang@biomed.wustl.edu.

References

- Nagy JA, Shih SC, Wong WH, Dvorak AM, Dvorak HF. The adenoviral vector angiogenesis/lymphangiogenesis assay. *Methods Enzymol.* 2008;444:43-64.
- Grunewald M, Avraham I, Dor Y, et al. VEGF-induced adult neovascularization: recruitment, retention, and role of accessory cells. *Cell.* 2006;124(1):175-189.
- Phung TL, Ziv K, Dabydeen D, et al. Pathological angiogenesis is induced by sustained Akt signaling and inhibited by rapamycin. *Cancer Cell.* 2006;10(2):159-170.
- Fukumura D, Jain RK. Imaging angiogenesis and the microenvironment. *APMIS.* 2008;116(7):695-715.
- Yan P, Bero AW, Cirrito JR, et al. Characterizing the appearance and growth of amyloid plaques in APP/PS1 mice. *J Neurosci.* 2009;29(34):10706-10714.
- Vakoc BJ, Lanning RM, Tyrrell JA, et al. Three-dimensional microscopy of the tumor microenvironment in vivo using optical frequency domain imaging. *Nat Med.* 2009;15(10):1219-1223.
- Rankin EB, Giaccia AJ. The role of hypoxia-inducible factors in tumorigenesis. *Cell Death Differ.* 2008;15(4):678-685.
- Schofield CJ, Ratcliffe PJ. Signalling hypoxia by HIF hydroxylases. *Biochem Biophys Res Commun.* 2005;338(1):617-626.
- Semenza GL. Targeting HIF-1 for cancer therapy. *Nat Rev Cancer.* 2003;3(10):721-732.
- Hickey MM, Simon MC. Regulation of angiogenesis by hypoxia and hypoxia-inducible factors. *Curr Top Dev Biol.* 2006;76:217-257.
- Elson DA, Thurston G, Huang LE, et al. Induction of hypervascularity without leakage or inflammation in transgenic mice overexpressing hypoxia-inducible factor-1alpha. *Genes Dev.* 2001;15(19):2520-2532.
- Tang N, Wang L, Esko J, et al. Loss of HIF-1alpha in endothelial cells disrupts a hypoxia-driven VEGF autocrine loop necessary for tumorigenesis. *Cancer Cell.* 2004;6(5):485-495.
- Du R, Lu KV, Petritsch C, et al. HIF1alpha induces the recruitment of bone marrow-derived vascular modulatory cells to regulate tumor angiogenesis and invasion. *Cancer Cell.* 2008;13(3):206-220.

14. Diamond I, Owolabi T, Marco M, Lam C, Glick A. Conditional gene expression in the epidermis of transgenic mice using the tetracycline-regulated transactivators tTA and rTA linked to the keratin 5 promoter. *J Invest Dermatol*. 2000;115(5):788-794.
15. Bekereldjian R, Walton CB, MacCannell KA, et al. Conditional HIF-1 α expression produces a reversible cardiomyopathy. *PLoS ONE*. 2010; 5(7):e11693.
16. Scortegagna M, Martin RJ, Kladney RD, Neumann RG, Arbeit JM. Hypoxia-inducible factor-1 α suppresses squamous carcinogenic progression and epithelial-mesenchymal transition. *Cancer Res*. 2009;69(6):2638-2646.
17. Lu K, Lamagna C, Bergers G. Bone marrow-derived vascular progenitors and proangiogenic monocytes in tumors. *Methods Enzymol*. 2008; 445:53-82.
18. Hu S, Maslov K, Wang LV. Noninvasive label-free imaging of microhemodynamics by optical-resolution photoacoustic microscopy. *Opt Express*. 2009;17(9):7688-7693.
19. Arbeit J. Transgenic models of epidermal neoplasia and multi-stage carcinogenesis. *Cancer Surv*. 1996;26:7-34.
20. Xia YP, Li B, Hylton D, Detmar M, Yancopoulos GD, Rudge JS. Transgenic delivery of VEGF to mouse skin leads to an inflammatory condition resembling human psoriasis. *Blood*. 2003;102(1): 161-168.
21. Thurston G, Suri C, Smith K, et al. Leakage-resistant blood vessels in mice transgenically overexpressing angiopoietin-1. *Science*. 1999; 286(5449):2511-2514.
22. Dan L, Shi-long Y, Miao-li L, et al. Inhibitory effect of oral doxycycline on neovascularization in a rat corneal alkali burn model of angiogenesis. *Curr Eye Res*. 2008;33(8):653-660.
23. Maslov K, Zhang HF, Hu S, Wang LV. Optical-resolution photoacoustic microscopy for in vivo imaging of single capillaries. *Opt Lett*. 2008;33(9): 929-931.
24. Gaengel K, Genove G, Armulik A, Betsholtz C. Endothelial-mural cell signaling in vascular development and angiogenesis. *Arterioscler Thromb Vasc Biol*. 2009;29(5):630-638.
25. Benjamin LE, Hemo I, Keshet E. A plasticity window for blood vessel remodelling is defined by pericyte coverage of the preformed endothelial network and is regulated by PDGF-B and VEGF. *Development*. 1998;125(9):1591-1598.
26. Bergers G, Song S. The role of pericytes in blood-vessel formation and maintenance. *Neuro-oncology*. 2005;7(4):452-464.
27. Laderoute KR, Alarcon RM, Brody MD, et al. Opposing effects of hypoxia on expression of the angiogenic inhibitor thrombospondin 1 and the angiogenic inducer vascular endothelial growth factor. *Clin Cancer Res*. 2000;6(7):2941-2950.
28. Duval M, Bedard-Goulet S, Delisle C, Gratton JP. Vascular endothelial growth factor-dependent down-regulation of Flk-1/KDR involves Cbl-mediated ubiquitination: consequences on nitric oxide production from endothelial cells. *J Biol Chem*. 2003;278(22):20091-20097.
29. Olszewska-Pazdrak B, Hein TW, Olszewska P, Carney DH. Chronic hypoxia attenuates VEGF signaling and angiogenic responses by down-regulation of KDR in human endothelial cells. *Am J Physiol Cell Physiol*. 2009;296(5):C1162-C1170.
30. Shen BQ, Lee DY, Gerber HP, Keyt BA, Ferrara N, Zioncheck TF. Homologous up-regulation of KDR/Flk-1 receptor expression by vascular endothelial growth factor in vitro. *J Biol Chem*. 1998;273(45): 29979-29985.
31. Witte L, Hicklin DJ, Zhu Z, et al. Monoclonal antibodies targeting the VEGF receptor-2 (Flk1/KDR) as an anti-angiogenic therapeutic strategy. *Cancer Metastasis Rev*. 1998;17(2):155-161.
32. Wu Y, Zhong Z, Huber J, et al. Anti-vascular endothelial growth factor receptor-1 antagonist antibody as a therapeutic agent for cancer. *Clin Cancer Res*. 2006;12(21):6573-6584.
33. Murdoch C, Giannoudis A, Lewis CE. Mechanisms regulating the recruitment of macrophages into hypoxic areas of tumors and other ischemic tissues. *Blood*. 2004;104(8):2224-2234.
34. Bergers G, Hanahan D. Modes of resistance to anti-angiogenic therapy. *Nat Rev Cancer*. 2008; 8(8):592-603.
35. Moore MA, Hattori K, Heissig B, et al. Mobilization of endothelial and hematopoietic stem and progenitor cells by adenovector-mediated elevation of serum levels of SDF-1, VEGF, and angiopoietin-1. *Ann N Y Acad Sci*. 2001;938:36-45, discussion 45-47.
36. Ceradini DJ, Kulkarni AR, Callaghan MJ, et al. Progenitor cell trafficking is regulated by hypoxic gradients through HIF-1 induction of SDF-1. *Nat Med*. 2004;10(8):858-864.
37. Mukherjee S, Tessema M, Wandinger-Ness A. Vesicular trafficking of tyrosine kinase receptors and associated proteins in the regulation of signaling and vascular function. *Circ Res*. 2006; 98(6):743-756.
38. Singh AJ, Meyer RD, Band H, Rahimi N. The carboxyl terminus of VEGFR-2 is required for PKC-mediated down-regulation. *Mol Biol Cell*. 2005; 16(4):2106-2118.
39. Gorgoulis VG, Vassiliou LV, Karakaidos P, et al. Activation of the DNA damage checkpoint and genomic instability in human precancerous lesions. *Nature*. 2005;434(7035):907-913.
40. Dickey JS, Redon CE, Nakamura AJ, Baird BJ, Sedelnikova OA, Bonner WM. H2AX: functional roles and potential applications. *Chromosoma*. 2009;118(6):683-692.
41. Economopoulou M, Langer HF, Celeste A, et al. Histone H2AX is integral to hypoxia-driven neovascularization. *Nat Med*. 2009;15(5):553-558.
42. To KK, Sedelnikova OA, Samons M, Bonner WM, Huang LE. The phosphorylation status of PAS-B distinguishes HIF-1 α from HIF-2 α in NBS1 repression. *EMBO J*. 2006;25(20):4784-4794.
43. Uemura A, Kusuhara S, Katsuta H, Nishikawa S. Angiogenesis in the mouse retina: a model system for experimental manipulation. *Exp Cell Res*. 2006;312(5):676-683.
44. Ozerdem U, Stallcup WB. Early contribution of pericytes to angiogenic sprouting and tube formation. *Angiogenesis*. 2003;6(3):241-249.
45. Morikawa S, Baluk P, Kaidoh T, Haskell A, Jain RK, McDonald DM. Abnormalities in pericytes on blood vessels and endothelial sprouts in tumors. *Am J Pathol*. 2002;160(3):985-1000.
46. Nehls V, Denzer K, Drenckhahn D. Pericyte involvement in capillary sprouting during angiogenesis in situ. *Cell Tissue Res*. 1992;270(3):469-474.
47. Andrae J, Gallini R, Betsholtz C. Role of platelet-derived growth factors in physiology and medicine. *Genes Dev*. 2008;22(10):1276-1312.
48. Hattori K, Dias S, Heissig B, et al. Vascular endothelial growth factor and angiopoietin-1 stimulate postnatal hematopoiesis by recruitment of vasculogenic and hematopoietic stem cells. *J Exp Med*. 2001;193(9):1005-1014.
49. Dineen SP, Lynn KD, Holloway SE, et al. Vascular endothelial growth factor receptor 2 mediates macrophage infiltration into orthotopic pancreatic tumors in mice. *Cancer Res*. 2008;68(11):4340-4346.
50. De Palma M, Venneri MA, Galli R, et al. Tie2 identifies a hematopoietic lineage of proangiogenic monocytes required for tumor vessel formation and a mesenchymal population of pericyte progenitors. *Cancer Cell*. 2005;8(3):211-226.
51. Shojaei F, Wu X, Malik AK, et al. Tumor refractoriness to anti-VEGF treatment is mediated by CD11b+Gr1+ myeloid cells. *Nat Biotechnol*. 2007;25(8):911-920.
52. Wang LV. Multiscale photoacoustic microscopy and computed tomography. *Nat Photonics*. 2009; 3(9):503-509.
53. Hu S, Rao B, Maslov K, Wang LV. Label-free photoacoustic ophthalmic angiography. *Optics Lett*. 2010;35:1-3.